STAR Note 411

Can Doubly Strange Dibaryon Resonances be Discovered at RHIC?

S. D. Paganis,[1] G. W. Hoffmann, R. L. Ray[2], J.-L. Tang and T. Udagawa

Department of Physics
The University of Texas at Austin, Austin, Texas 78712

R. S. Longacre

Physics Department, Brookhaven National Laboratory, Upton, NY 11973

Abstract

The baryon-baryon continuum invariant mass spectrum generated from ultrarelativistic nucleus + nucleus collision data may reveal the existence of doubly-strange dibaryons not stable against strong decay if they lie within a few MeV of threshold. Furthermore, since the dominant component of these states is a superposition of two color-octet clusters which can be produced intermediately in a color-deconfined quark-gluon plasma (QGP), an enhanced production of dibaryon resonances could be a signal of QGP formation. A total of eight, doubly-strange dibaryon states are considered for experimental search using the STAR detector (Solenoidal Tracker at RHIC) at the new Relativistic Heavy Ion Collider (RHIC). These states may decay to $\Lambda\Lambda$ and/or $p\Xi^-$, depending on the resonance energy. STAR's large acceptance, precision tracking and vertex reconstruction capabilities, and large data volume capacity, make it an ideal instrument to use for such a search. Detector performance and analysis sensitivity are studied as a function of resonance production rate and width for one particular dibaryon which can directly strong decay to $p\Xi^-$, but not $\Lambda\Lambda$. Results indicate that a window of opportunity exists for discovery of such resonances using STAR if the resonance production rates are comparable to coalescence model predictions for dibaryon bound states.

[1]Present address: Nevis Laboratories, Columbia University, P. O. Box 137, Irvington, NY 10533.

[2]Corresponding author: electronic address: ray@physics.utexas.edu

1 Introduction

The only bound systems of quarks and gluons which have been observed are baryons, antibaryons and mesons. However, a number of models based on quantum chromodynamics (QCD) predict other types of quark and gluonic systems such as pure gluonic states (glueballs), hybrids ($q\bar{q}g$), four quark di-mesons ($qq\bar{q}\bar{q}$, $q\bar{q}q\bar{q}$) [1], penta-quark states ($qqqq\bar{q}$), six quark dibaryons [2], strangelets, and for large systems several fm in size at sufficiently high temperature and/or net baryon density, the color-deconfined quark-gluon plasma (QGP). Extensive experimental searches have been made for all these systems.

In particular, many experiments (*e.g.* [3, 4, 5]) have searched for a stable (at least to strong decay), doubly-strange flavor-singlet dibaryon (H_0) of the six quark SU(3)-flavor [$SU(3)_f$] multiplets [6]. This hypercharge (Y) = 0 dibaryon was predicted by Jaffe [2] to be stable against strong decay, but not to weak decay; hence the experiments generally searched for characteristic weak decay topologies. So far, no conclusive evidence for a bound H_0 has been presented [3, 4, 5]. However, the H_0 mass may be larger than $M_{\Lambda\Lambda} \equiv M_\Lambda + M_\Lambda$, the $\Lambda\Lambda$ strong decay threshold [7, 8, 9]. In this case the H_0 could be a strong interaction resonance. If the resonance lies only a few MeV above $M_{\Lambda\Lambda}$, then it may be possible to see experimental evidence for its existence[3] [7]. In addition, it is important to point out that several other doubly-strange dibaryon states occur in the $SU(3)_f$ multiplets which do not directly strong decay to $\Lambda\Lambda$ and which may also appear as resonances in the $\Lambda\Lambda$ and $N\Xi$ systems.

Experimental searches for a stable H_0 have attempted to create and observe the H_0 through: (1) double-strangeness-exchange reactions, such as $A(K^-, K^0)X$, $A(K^-, K^+)X$; (2) $\Xi^- A$ capture [3] on nuclear targets with $A \geq 2$; and (3) proton + nucleus [4, 5] or nucleus + nucleus collisions where the H_0 production mechanism could proceed via multi-hyperon production followed by coalescence [10, 11, 12]. Reactions such as $d(K^-, K^0)H_0$, for example, produce a relatively clean final state but suffer from poor momentum matching and subsequently, a reduced production rate. Heavy ion collisions, although producing a complex final state, generate a large number of co-moving hyperons and non-strange baryons from which dibaryons could either coalesce or scatter through resonances. The invariant mass spectrum for $\Lambda\Lambda$ pairs produced in 158 A GeV/c Pb + Pb collisions [data from WA97 [13]] does not reveal any resonance like structures. However, the data are too coarsely binned and lack sufficient statistics to be relevant for the type of experimental search proposed here.

The Relativistic Heavy Ion Collider (RHIC) facility at the Brookhaven National

[3] In the meson sector nature provides several examples of narrow states that lie a few MeV above their strong decay thresholds. The $\phi(1020)$, $D^*(2010)^\pm$, $D^*(2007)^0$ and $D_{S1}(2536)^+$ mesons are 32.1, 5.8, 7.1 and 35.0 MeV, respectively, above their strong decay thresholds and have total widths of 4.4, <0.13, <2.1 and <2.3 MeV, respectively. The latter three quantities represent upper limits at the 90% confidence level.

Laboratory, together with four new detectors, is beginning a program of research whose primary goal is to produce a quark-gluon plasma and study its properties. It is noteworthy that a color-deconfined QGP could enhance significantly the production of H_0 dibaryons compared to the production expected from a hot hadronic gas [11]. The reason is that the largest component of the six quark dibaryon wave function consists of a color-singlet superposition of color-octet-octet components [7, 11, 14]:

$$|H\rangle = \sqrt{\frac{1}{5}}\,|BB\rangle + \sqrt{\frac{4}{5}}\,|8_c \otimes 8_c\rangle \ . \tag{1}$$

Here, $|8_c \otimes 8_c\rangle$ represents the color-octet-octet components, and $|BB\rangle$ denotes a summation of states composed of two physical baryons. Enhanced dibaryon production can occur by way of fusion of color-octet clusters within the deconfined plasma [11]. If evidence for dibaryon resonances is observed in the data from RHIC collisions, then analyses of such data would provide an independent basis for studying the QGP.

In this work we explore the feasibility of observing evidence for the existence of several doubly-strange dibaryon *resonances* through study of the $\Lambda\Lambda$ and $N\Xi$ invariant mass spectra constructed from relativistic heavy ion collision data to be taken at RHIC.[4] We focus on using the STAR [15] detector [with the Silicon Vertex Tracker (SVT) and Silicon Strip Detector (SSD) [16] upgrades] since it is the most suited of the RHIC detectors for such a program. A preliminary study [16] suggested that STAR could be used to search for $H_0 \to \Lambda\Lambda$ with resonance masses a few hundred MeV above $M_{\Lambda\Lambda}$. The focus of the present work is on the $N\Xi$ decay channel with resonance masses a few MeV above the strong decay threshold.

In Sec. 2 the doubly-strange dibaryons and their possible decay schemes are discussed. Using the P-matrix formalism [7] the resonance widths are estimated in Sec. 3. In Sec. 4 the $J^\pi = 0^+$, I(isospin) = 1, $I_3 = 0$ dibaryon member of the $SU(3)_f$ **27**-plet [6] [referred to as $H^{27}(J^\pi,I,I_3)$ with $J^\pi = 0^+$, I = 1 and $I_3 = 0$], which cannot directly strong decay to $\Lambda\Lambda$, is used to explore the sensitivity of analysis of STAR data to the existence of such resonances, if they exist. A new, fast simulation detector response code (FSDR) is used for this study. Finally, a summary and conclusions are presented in Sec. 5.

[4] Formation of hyper-nuclear baryon-baryon bound states or slightly unbound states is also possible (*e.g.* strange baryon analogs of the deuteron and the nucleon + nucleon $^1S_0$ unbound state). Such states, if they exist, are expected to produce broad enhancements over many tens of MeV in the $\Lambda\Lambda$ or $N\Xi$ spectra, and not the narrow resonance structures predicted for six quark states which are the focus of the present work.

2 Dibaryon States

The direct product space of the $J^\pi = \frac{1}{2}^+$ baryon octet with itself can be written in terms of irreducible representations of SU(3)$_f$ [6]:

$$\mathbf{8} \otimes \mathbf{8} = \mathbf{1} \oplus \mathbf{8} \oplus \mathbf{8} \oplus \mathbf{10} \oplus \overline{\mathbf{10}} \oplus \mathbf{27}. \quad (2)$$

The hypercharge (Y) ranges from +2 (NN, nucleon-nucleon) to −2 ($\Xi\Xi$) for these dibaryon states. The $Y = 2$ members include the deuteron of the $\overline{\mathbf{10}}$-multiplet. The $Y = 1$ states contain NΛ and NΣ components. Sharp enhancements in the NΛ spectra at 2129 MeV [17] [the NΣ threshold [18, 19]] and 2139 MeV [18] have been observed in single strangeness-exchange reactions such as d(K, π)X and d(π, K)X. The Y= −1 and −2 states contain the experimentally difficult $\Xi\Lambda$, $\Xi\Sigma$ and $\Xi\Xi$ components. Finally, the $Y = 0$ dibaryons contain $\Lambda\Lambda$, $N\Xi$, $\Lambda\Sigma$, and $\Sigma\Sigma$ components. Since Ns, Λs, Σs, and Ξs are produced in relativistic heavy ion $A+A$ central collisions, the RHIC experiments will provide an excellent opportunity to search for some of these $Y = 0$ dibaryons.

Table I lists the $J^\pi = 0^+, 1^+$ $Y = 0$ dibaryon constituents of the various SU(3)$_f$ multiplets in Eq. (2) from Refs. [2, 6] along with the dominant decay modes for a wide range of assumed dibaryon masses. The mass limits where strong and/or electromagnetic (EM) decay channels open are noted for each state. In general the best mass ranges to explore for resonances are those lying just above the strong and/or EM decay thresholds in Table I. Jaffe [2] predicted a significant increase in the dibaryon masses with increasing dimensionality of the SU(3)$_f$ representation. However, more recent calculations based on QCD sum rules [20, 21] indicate that the $Y = 0$ dibaryons in different multiplets should be similar in mass; the principal mass dependence of the $\mathbf{8}\otimes\mathbf{8}$ dibaryons is due to the explicit SU(3)$_f$ symmetry breaking caused by the strange quark mass.[5] All of the $Y = 0$ dibaryon states in Table I will be considered in this work, since at present there is no reason to exclude them from experimental searches.

For masses between M$_{\Lambda\Lambda}$ and M$_{N\Xi}$ the singlet H$_0$ and H$^{27}(0^+, 0, 0)$ can strong decay to $\Lambda\Lambda$. Recently, using a P-matrix formalism, Bashinsky and Jaffe [7] considered a hypothetical singlet H$_0$ strong-decay resonance of mass several MeV above the $\Lambda\Lambda$ (strong decay) threshold. For a variety of assumptions, they found that, owing to kinematic effects near threshold, the cross sections for S-wave $\Lambda\Lambda$ elastic scattering should show structures whose scales are of the order of several MeV. One can speculate that the $\Lambda\Lambda$ invariant mass spectrum generated from relativistic heavy ion collision data may show similar structure that may be taken as evidence of the existence of such a resonance. The analysis in [7] also applies for the H$^{27}(0^+, 0, 0)$ case.

[5] It is also worth noting that the $Y = 2$ deuteron member of the $\overline{\mathbf{10}}$-flavor multiplet and the nucleon + nucleon ^{1}S$_0$ unbound state member of the **27**-flavor multiplet differ in mass by only a few MeV. Calculations [19] based on a SU(3) invariant pseudoscalar and vector meson exchange model for the baryon-baryon system predict the 0^+ **27**-plet dibaryon mass to be less than the mass of the singlet H$_0$.

The **8**-, **10**- and $\overline{\mathbf{10}}$-plet $J^\pi = 1^+$ dibaryons and the $H^{27}(0^+, 1, I_3)$ and $H^{27}(0^+, 2, I_3)$ dibaryons cannot strong decay to $\Lambda\Lambda$ since antisymmetrization requires the final $\Lambda\Lambda$ system to be spin-singlet-even or spin-triplet-odd and I($\Lambda\Lambda$)=0. The $H^{27}(0^+, 1, 0)$ and $H^{27}(0^+, 2, 0)$ dibaryons can, however, strong decay to $\Lambda\Lambda$ by way of the small I=0 isospin admixture which contributes to the physical states due to Coulomb induced isospin mixing, but this transition rate should be much less than that for $H_0 \to \Lambda\Lambda$. The four $J^\pi = 1^+$, I_3=0 states can EM decay to $\Lambda\Lambda\gamma$ via E1 transitions leaving the $\Lambda\Lambda$ in relative ^3P_J states. The $H^{27}(0^+, 1, 0)$ and $H^{27}(0^+, 2, 0)$ states can also EM decay to $\Lambda\Lambda\gamma$, for example via E1 transition to the $^3P_1$ $\Lambda\Lambda$ final state. All remaining states (*i.e.,* those with $I_3 \neq 0$) in this mass range (from $M_{\Lambda\Lambda}$ to $M_{N\Xi}$) can decay only weakly. It is likely that the $J^\pi = 1^+$ states are of larger mass than the 0^+ states and thus even more difficult to deal with experimentally.

In the mass range from $M_{N\Xi}$ to $M_{\Sigma\Sigma}$ all states with $I < 2$ decay strongly to $\Lambda\Lambda$, $N\Xi$ or $\Lambda\Sigma$ as indicated in Table I. The $H^{27}(0^+, 2, \pm 1)$ [$H^{27}(0^+, 2, 0)$] states can strong decay to $N\Xi$ and $\Lambda\Sigma$ [$N\Xi$, $\Lambda\Sigma$ and $\Lambda\Lambda$] via isospin admixtures or they can decay electromagnetically. The $H^{27}(0^+, 2, \pm 2)$ remain blocked to both strong and EM decays up to $M_{\Sigma\Sigma}$ due to charge conservation. The $H^{27}(0^+, 1, I_3)$ members of the **27**-multiplet cannot strong decay to $\Lambda\Lambda$ because of isospin conservation; however, they can strong decay to $N\Xi$ and $\Lambda\Sigma$ if the mass is greater than $M_{N\Xi}$ and $M_{\Lambda\Sigma}$, respectively. Above $M_{\Sigma\Sigma}$ all states in Table I can decay strongly.

Table II lists the optimum decay channels and mass ranges for possible $Y = 0$ dibaryon resonance searches. The last column indicates whether the channels include those appropriate for STAR [15]. Of the listed decay products, STAR can identify only protons (p), Λs and Ξ^-s. Eight of the $Y = 0$ dibaryon states in Tables I and II (corresponding to each of the I_3=0 states) are seen to be appropriate for a program of research with STAR.

Evidence for the H_0 and $H^{27}(0^+, 0, 0)$ states might be seen in the $\Lambda\Lambda$ invariant mass spectrum within several MeV of threshold. The four $J^\pi = 1^+$, I_3=0 states, if in the mass range from $M_{\Lambda\Lambda}$ to $M_{n\Xi^0}$, will decay electromagnetically to $\Lambda\Lambda\gamma$. If the photon is not detected, the $\Lambda\Lambda$ invariant mass spectrum would appear as a broad continuum. However, an enhancement still might be observed if the resonance masses are only a few MeV above $M_{\Lambda\Lambda}$. These four resonances might also be observed in the $p\Xi^-$ spectrum if either lies just above the $M_{p\Xi^-} = 2259.6$ MeV strong breakup threshold.[6]

If the resonance mass exceeds $M_{\Lambda\Lambda}$, the $H^{27}(0^+, 1, 0)$ and $H^{27}(0^+, 2, 0)$ states can decay either electromagnetically to $\Lambda\Lambda\gamma$ or strongly via the small I=0 admixture. The competition between these branches determines the experimental signature. If the strong interaction, isospin admixture decay dominates the EM decay, then the I=1(2) state might be observed if its mass is between $M_{\Lambda\Lambda}$ and $M_{n\Xi^0}$ ($M_{\Sigma^0\Sigma^0}$).

[6]Due to Coulomb interactions the $n\Xi^0$ and $p\Xi^-$ mass thresholds are split by 5.1 MeV. Strong decay to $N\Xi$ therefore opens at $M_{n\Xi^0}$=2254.5 MeV, whereas the observable decay channel for STAR, dibaryon$\to p\Xi^-$, does not open until 2259.6 MeV.

If the EM decay dominates, then both I=1 and 2 states might only be observed as enhancements in the continuum just above $M_{\Lambda\Lambda}$. Otherwise the $H^{27}(0^+,1,0)$ state might be seen in the $p\Xi^-$ invariant mass spectrum just above the $M_{p\Xi^-}$ threshold. In this case $H^{27}(0^+,1,0) \rightarrow p\Xi^-$ might be observable with STAR. The $H^{27}(0^+,2,0)$ resonance could strong decay to $\Sigma^0\Sigma^0$ and $\Sigma^+\Sigma^-$ final states, but the Σs, unfortunately, cannot be reconstructed by STAR.

In this initial simulation study we prefer to consider the dibaryon resonance with smallest angular momentum which may strong decay to $p\Xi^-$ but not to $\Lambda\Lambda$, namely $H^{27}(0^+,1,0)$. The reason for this choice is the expectation that the combinatoric background contribution to the $p\Xi^-$ invariant mass spectrum will be less than that for $\Lambda\Lambda$ for the case of RHIC data for Au + Au central collisions (see Sec. 4.) Simulation studies for the remaining dibaryon resonances in Table II will be done in the future.

It is worth noting that threshold-cusp effects [18, 19] could produce enhancements in the $\Lambda\Lambda$ spectra at the $N\Xi$, $\Sigma\Sigma$, etc., thresholds, independent of any possible resonances. This is also true for the $N\Xi$ spectra (I=1 component) at the $\Lambda\Sigma$ and $\Sigma\Sigma$ thresholds. Such enhancements are due to coupled-channels scattering effects near inelastic thresholds and must be treated carefully when searching for experimental evidence of dibaryon resonances.

Resonances occuring between the $n\Xi^0$ and $p\Xi^-$ thresholds will decay primarily to $n\Xi^0$, although decay to $p\Xi^-$ will occur if the resonance width is such that the distribution extends above $M_{p\Xi^-}$. For resonance masses near or a few MeV above $M_{p\Xi^-}$, the branching ratio between the $n\Xi^0$ and $p\Xi^-$ channels depends upon the dynamics of the $n\Xi^0 - p\Xi^-$–dibaryon coupled channels system, as well as on the kinematic density of final states factor. For resonance energies much above $M_{p\Xi^-}$ the branching ratio is determined mainly by isospin invariance which results in a 50% decay fraction for both channels. Thus the study in Sec. 4 will be in terms of the dibaryon resonance width and production rate for the observable dibaryon$\rightarrow p\Xi^-$ decay channel only. Inclusion of the model-dependences associated with the $n\Xi^0 - p\Xi^-$–dibaryon system lies well beyond the scope and purpose of this work.

Finally, we note that the decay products of resonance states formed deep within the interior of the collision region will undergo strong, final state interactions (FSI) so that observation of these resonances becomes more difficult. It is likely that only resonances occuring in the periphery of the QGP or in the mixed QGP-hadronic phase prior to freeze-out will lead to experimental signatures in invariant mass spectra. Detailed calculations of FSI effects on this and other potential QGP signals remain to be done.

3 Dibaryon Resonance Widths

Bashinsky and Jaffe [7] used the P-matrix scattering formalism to compute the $\Lambda\Lambda$ elastic scattering S-wave total cross section in the presence of a flavor-singlet,

H_0 dibaryon resonance located a few MeV above the $\Lambda\Lambda$ threshold. Their model is used in this section for the similar case of a possible $H^{27}(0^+,1,0)$ (for brevity referred to as H^{27} in the remainder of this paper) dibaryon resonance lying just above the $N\Xi$ threshold.

The total cross section for $N\Xi$ elastic scattering is given by

$$\sigma_{\rm TOT} = \frac{4\pi}{k_1}{\rm Im}(f_{11}) \quad , \tag{3}$$

where f_{11} is approximated by the forward, S-wave elastic scattering amplitude, which in the P-matrix formalism is written as [7]

$$f_{11} = \frac{1}{\frac{1}{K_1^{(red)}} - ik_1}. \tag{4}$$

The reduced K-matrix from Ref. [7] as a function of total energy (ϵ) in the $N\Xi$ channel is

$$K_1^{(red)}(\epsilon) \simeq -\overline{a}_1' - \frac{\rho_1'/2m}{\epsilon - \epsilon_{th1} - \epsilon_1'} \quad , \tag{5}$$

where,

$$\overline{a}_1' = \frac{\overline{a}_1}{1-\rho_1 b_0}, \rho_1' = \rho_1 \frac{1-\rho_1 b_0 + 2m\epsilon_r \overline{a}_1 b_0}{(1-\rho_1 b_0)^2}, \epsilon_1' = \frac{\epsilon_1}{1-\rho_1 b_0} \quad . \tag{6}$$

In Eqs. (3)-(6), k_1 is the relative center-of-momentum system wave number, m is the reduced mass of the two-baryon ($N\Xi$) system, ϵ_{th1} is the $N\Xi$ threshold energy, ϵ_r is the assumed resonance mass of the H^{27} dibaryon, and $\epsilon_1 = \epsilon_r - \epsilon_{th1}$. Parameter b_0 is a resonance size parameter with typical value (150 MeV)$^{-1}$, ρ_1 is the resonance width parameter which is a function of the resonance state - decay channel coupling, and $\overline{a}_1$ is the $N\Xi$ scattering length which was assumed to be (200 MeV)$^{-1}$.

Elastic total cross section results obtained using Eqs. (3)-(6) are shown in Fig. 1 by the solid lines for assumed values of ϵ_1 = 2, 3 and 5 MeV and for the typical resonance width parameter ρ_1=50 MeV. The unitarity limit, $4\pi/k_1^2$, is indicated by the dashed lines. These results indicate that the resonance distribution displays a characteristic width roughly proportional to the difference between the resonance and threshold energies.

Resonances decaying to $p\Xi^-$ may also decay to $n\Xi^0$ which is 5.1 MeV lower in energy. These results suggest that resonances near $M_{p\Xi^-}$ would be about 5 MeV wide. It is reasonable to assume, however, that the $p\Xi^-$ spectra for such cases would display a narrower range of enhancement because of the kinematic limit which cuts off the lower energy portion of the $p\Xi^-$ invariant mass distribution.

4 Search for Dibaryon Resonances using STAR

An environment conducive to the formation of dibaryon resonances may be the hot, dense nuclear matter that will be created through ultrarelativistic, central Au + Au collisions at RHIC. The experimental objective, then, is to infer evidence for the existence of such resonances through examination of $\Lambda\Lambda$ or $p\Xi^-$ invariant mass spectra. Since the resonance cross sections are expected to be small, a large acceptance detector with the ability to do precision tracking to within a few cm of the production vertex is required. In addition, the detector must handle high data rates and have event processing capabilities for very large data volumes. The STAR detector [15] at RHIC with its central vertex tracking system (SVT-SSD) is well-suited for such experiments. For the simulations to be discussed here, the parameters in Table III were used to approximate the kinematic acceptance and reconstruction performance of STAR (including the SVT-SSD). The momentum resolution and track reconstruction efficiencies were taken from previous simulation studies [16, 22].

Coalescence model calculations [11] for Au+Au central collisions at AGS energies ($\sim$11 A$\cdot$GeV fixed target) predict of order 0.1 to 0.5 flavor-singlet H_0s per event, depending on the assumed temperature and strangeness content of the hadron gas. Color-deconfinement in the QGP could further enhance the production rate via the color-octet-octet component of the dibaryon wave function [Eq. (1)]. At RHIC energies increased strangeness production and possible QGP formation could enhance the dibaryon production rate above this range. Source expansion and collective flow in RHIC collisions could also affect coalescence model predictions [12]. Comprehensive calculations including all these effects have not been done. Nevertheless, the results of such calculations suggest the necessary level of sensitivity for the experimental search to be meaningful.

In the following, analytical estimates are presented for the dibaryon resonance signal-to-background ratio for cases of interest. The number of Au+Au central RHIC collision events at STAR required to achieve reasonable statistics in the $p\Xi^-$ invariant mass spectra is estimated. This is followed by a description of a fast numerical simulation model and presentation of sensitivity results for experimental detection of a hypothetical, narrow dibaryon resonance in the $p\Xi^-$ channel just above threshold.

Analytical Estimates

For these estimates only that portion of the $p\Xi^-$ invariant mass spectrum just above threshold ($\sim$2259.6 MeV) is considered. Note that for $p\Xi^-$ with invariant mass 7 MeV above threshold the relative p-Ξ^- momentum difference is 175 MeV/c. Thus, momentum resolution effects (Table III) do not significantly degrade the dibaryon resonance peak if the intrinsic width is a few MeV. For example, finite momentum resolution [22] for the final, reconstructed daughter protons and π^-s in the decay chain, dibaryon $\rightarrow p\Xi^- \rightarrow p(\Lambda\pi^-) \rightarrow p(p\pi^-)\pi^-$, results in about

10 MeV/c uncertainty for the p-Ξ^- relative momentum. A resonance with an intrinsic width of 2 MeV (Gaussian σ) would lead to a width of approximately 2.7 MeV in the experimentally reconstructed $p\Xi^-$ invariant mass distribution as a result of finite momentum resolution effects.

The integrated signal-to-background ratio for the $p\Xi^-$ invariant mass distribution can be approximated by the expression

$$R = \frac{n_H}{[(n_H + n_{th\Xi})(1 + n_{F\Xi}/n_{R\Xi})(n_H + n_{thp})(1 + n_{Fp}/n_{Rp}) - n_H]B} \ , \qquad (7)$$

where n_H is the assumed number of dibaryon resonances per Au + Au central event that decay to $p\Xi^-$ into the kinematic acceptance range specified in Table III, $n_{th\Xi}$ and n_{thp} are the numbers of thermal Ξ^-s and protons, respectively, produced in the fireball within the acceptance per event, and the quantities $(n_{F\Xi}/n_{R\Xi})$ (*i.e.* number of reconstructed false Ξ^- divided by the number of correctly reconstructed Ξ^-) and (n_{Fp}/n_{Rp}) (similar definition except for reconstructed protons) are the integrated background to integrated signal ratios for the reconstructed Ξ^-s and protons, respectively. B is defined as

$$B = \frac{N(p\Xi^-)}{N_{\rm TOT}(p)N_{\rm TOT}(\Xi^-)} \ , \qquad (8)$$

where $N(p\Xi^-)$ is the number of uncorrelated p-Ξ^- pairs having invariant mass in the specified range, and $N_{\rm TOT}$ are the total number of protons or Ξ^-s within the acceptance.

Eqs. (7) and (8) were used to estimate the integrated signal-to-background ratios in central Au + Au collisions at RHIC energies for a $p\Xi^-$ dibaryon resonance 1 MeV above threshold with a 2 MeV width (Gaussian σ). The integration range included $p\Xi^-$ invariant masses from 2260 to 2267 MeV (*i.e.* from threshold to the resonance mass plus 3σ). The assumed values of n_H were 0.01, 0.1, 1 and 10. The quantity $(n_{F\Xi}/n_{R\Xi})$ was assumed to be either 5.6 based on the present simulations which used relaxed vertex reconstruction cuts (see following discussion) or 1.5 based on previous simulation studies [23] which used more stringent vertex reconstruction cuts. The numbers of Ξ^-s and protons, $n_{th\Xi}$ and n_{thp}, were assumed to be 1.6 and 40 per event, respectively [12, 24, 25, 26, 27, 28]. The number of false reconstructed protons should only be a few percent; (n_{Fp}/n_{Rp}) was therefore taken to be 0.05. The value of B was determined using model representations of the proton and Ξ^- distributions [29] from VENUS [25]. For the invariant mass range from 2260 to 2267 MeV B equals 0.0072. With these parameters R in Eq. (7) equals 0.003, 0.03, 0.18 and 0.34 (0.008, 0.07, 0.5 and 0.9) for $n_H = 0.01$, 0.1, 1 and 10, respectively, assuming relaxed (stringent) cuts in the Ξ^- reconstruction. These values are consistent with simulation results that follow. Sensitivity to the presence of dibaryon resonances is roughly proportional to the signal-to-background ratio for the reconstructed Ξ^-s, provided one can maintain ample statistics.

From the preceding estimates of $n_{th\Xi}$, n_{thp}, $(n_{F\Xi}/n_{R\Xi})$, (n_{Fp}/n_{Rp}) and B together with the proton track finding efficiency (Table III) and Ξ^- reconstruction

efficiencies (see following discussion) the number of reconstructed $p\Xi^-$ pairs per central Au + Au RHIC collision event at STAR in the invariant mass range from 2260 to 2267 MeV is estimated to be 0.19 (0.0024) assuming relaxed (stringent) cuts for the Ξ^- reconstruction. Thus about 4K (with relaxed cuts) [300K (with stringent cuts)] Au + Au central events are required in order to achieve $\sim$10% statistics in 1 MeV bins for this $p\Xi^-$ invariant mass range. This corresponds to about an hour (with relaxed cuts) [3 to 4 days (with stringent cuts)] of STAR data acquisition. Obtaining a statistically accurate $p\Xi^-$ spectrum, even with stringent reconstruction requirements, is well within the capabilities of the STAR experiment.

Numerical Simulations

A fast simulation detector response code (FSDR) was developed to provide rapid evaluation of the capabilities of relativistic heavy ion experiments with respect to proposed new measurements and research programs. In simplest terms, FSDR projects a given input list of particles from an event generator directly to the final, reconstructed particle list. Specific detector acceptance and track reconstruction performance parameters are supplied from realistic simulations and analyses. The values assumed for STAR are listed in Table III [16, 22, 23]. FSDR propagates (freely) and decays unstable particles such as Λ and Ξ^- according to known branching ratios and lifetimes and applies acceptance cuts, track finding efficiencies, particle identification efficiencies, and momentum resolution smearing to the charged primary particles and to the charged daughter particles from the decays.

Following this, FSDR reconstruction of Λ and Ξ^- is very similar to that used in the actual STAR reconstruction analysis. The charged particles selected for this analysis were assumed to be reconstructed in both the SVT-SSD and TPC (Time Projection Chamber). The SVT-SSD provides excellent track position resolution (few tens of microns) [16, 22] in the decay region within several cm of the primary vertex. Reconstructed trajectories (assumed to be helices) were projected to the primary vertex where an impact parameter cut (1 mm) differentiated primary particles (*i.e.,* those assumed to emerge from the primary collision vertex) from secondary particles (*i.e.,* those assumed to come from decay vertices). Candidate Λ decays were found by a distance of closest approach (DCA) cut (2 mm) among the projected trajectories of the secondary protons and π^-s. The resulting Λ reconstruction in the $p\pi^-$ invariant mass spectrum is shown in Fig. 2 for 600 central Au + Au HIJET collision events which included an average of 6.6 $H^{27} \rightarrow p\Xi^- \rightarrow p(\Lambda\pi^-)$ embedded decays per event (see following discussion). The cross-hatched region indicates the number of reconstructed $p-\pi^-$ pairs actually produced by Λ decays in the simulation. The reconstruction efficiency for primary Λs (*i.e.* number correctly reconstructed divided by number in acceptance) obtained here was about 5-6%,[7] in reasonable agreement with the 8% value in Ref. [23] and the range of

[7] The reconstruction efficiency for Λs from Ξ^- decays is somewhat higher than that for primary

$4-15\%$ in Ref. [16]. The $\pm 3\sigma$ width of the reconstructed Λ peak in Fig. 2 is about 8 MeV which quantitatively agrees with that found in Ref. [23]. Further cuts could reduce the background for primary Λs as in Ref. [23], but this was not done here in order to retain the secondary Λs from Ξ^- decays.

A DCA cut (4 mm) among all pairs of selected Λ candidates [*i.e.,* those with impact parameter less than 2 cm from the primary vertex and which have a reconstructed mass within $\pm 3\sigma$ (± 4 MeV) of the peak in Fig. 2] with all remaining secondary π^-s yielded the Ξ^- spectrum shown in Fig. 3 using the same events as in Fig. 2. The cross-hatched region indicates Λ and π^- reconstructed pairs that originate from Ξ^- decays. The FSDR Ξ^- reconstruction efficiency with the preceding cuts was about 0.06 which is larger than that in Ref. [23]. The higher reconstruction efficiency obtained here is offset by the smaller peak signal-to-background ratio here ($\sim \frac{1}{4}$) compared to the larger value (~ 1) in Ref. [23]. The $\pm 3\sigma$ width of the reconstructed Ξ^- peak in Fig. 3 is about 10 MeV, in good agreement with Ref. [23]. A tight selection of primary protons (impact parameter from primary vertex $\leq 100\mu$m) and Ξ^- candidates (within ± 6 MeV of the peak in Fig. 3) with projected DCAs ≤ 6 mm, provided the set of $p\Xi^-$ pairs used in the invariant mass plot in Fig. 4.

Variable numbers of H^{27} resonances were randomly embedded in the HIJET [28] event generator output for 200 A·GeV Au+Au central collisions according to the following distribution,

$$\frac{dN}{dp^3} = A\mathrm{e}^{-m_T/T}\mathrm{e}^{-\beta m_T \cosh(y)}. \tag{9}$$

In Eq. (9) $m_T = \sqrt{M(H^{27})^2 + p_T^2}$ is the transverse mass, $T = 238$ MeV, $\beta = 3.0$ GeV^{-1}, A is a normalization constant, and at midrapidity (y=0) the m_T distribution corresponds to an effective temperature of 139 MeV. For this distribution function approximately 39% of the total H^{27}s have all four decay particles fully contained within the acceptance (Table III). In the following discussion, production rates refer to the number of $H^{27} \rightarrow p\Xi^-$ decays per event for which all four decay particles are within the STAR acceptance. In FSDR the H^{27} masses were randomly distributed according to a Gaussian distribution where the resonance mass was placed 1 MeV above threshold and the width (σ) was varied from 0.3 to 3.0 MeV. Random throws which yielded masses less than threshold were discarded. For each value of $H^{27} \rightarrow p\Xi^-$ production rate and resonance width, a set of 500 – 1000 simulated Au+Au central RHIC events was analyzed.

The $p\Xi^-$ invariant mass spectrum that resulted from the simulation is shown in Fig. 4 for 600 Au+Au central collision events for an H^{27} resonance with 2 MeV width (σ) and an average production rate per event of 6.6 (total) or 2.6 into the STAR acceptance as defined in Table III. The cross-hatched portion of the spectrum corresponds to $p\Xi^-$ reconstructed pairs from actual H^{27} decays. The

Λs since the decay vertices are distributed farther from the primary vertex where the proton and π^- daughters are not as likely to be removed by the 1 mm impact parameter cut as occurs for the daughter tracks from primary Λ decays.

background subtracted peak is shown in the inset panel where the background was fitted with a fifth-order polynomial. The H^{27} peak is quite apparent for this case when the resonance occurs near threshold, where the background is rapidly decreasing. The contributions of the large number of false Ξ^-s (see Fig. 3) are dispersed throughout the spectrum.

If we arbitrarily state that the peak-to-background ratio in the subtracted spectra must be at least 3:1 to clearly identify a dibaryon resonance, then we can vary the H^{27} width and $H^{27} \rightarrow p\Xi^-$ production rate to explore STAR's ability to *see* such resonances. Fig. 5 summarizes the results of such a study. For example, for a Gaussian width of 2 MeV, 1.1 $H^{27} \rightarrow p\Xi^-$ resonance decays into the STAR acceptance must occur per event in order to be detected.

The preceding method for detecting possible dibaryon resonances is fairly conservative. Normalized, mixed event pairs of $p-\Xi^-$ could also be used to construct an accurate and realistic background analogous to what is done in two-pion interferometry analyses [30]. This method should improve the sensitivity for detecting the presence of broad enhancements in the $p\Xi^-$ invariant mass spectra.

5 Summary and Conclusions

The possibility that $Y = 0$ dibaryon states may occur as narrow resonances, if located in energy just above the strong interaction breakup threshold, offers interesting new discovery opportunities for the relativistic heavy ion physics program at RHIC, especially for the STAR experiment. In the baryon octet $\otimes$ octet direct product space for $Y = 0$ dibaryons we have listed eight possible states (corresponding to I_3=0) which could, in principle, be discovered by STAR with its SVT-SSD central vertex tracking system. If produced, these I_3=0 states decay to $\Lambda\Lambda$ and/or $p\Xi^-$ channels, depending on the resonance energy. In addition, the formation of these resonances may be significantly enhanced in a color-deconfined medium, such as the QGP, by way of the dominant color-octet-octet component of the dibaryon wave function. A significant change in the production rate of these states, in conjunction with other QGP signals, would provide strong corroborative evidence for QGP formation. High quality statistics for the $p\Xi^-$ invariant mass spectrum can be expected at STAR with the analysis of data from of order several hundred thousand central Au+Au collision events — several days of STAR data acquisition.

One specific $Y = 0$ dibaryon state was used to illustrate and estimate the detection and sensitivity range of STAR. This state, the $J^\pi = 0^+$, I=1, I_3=0 member of the **27**-plet, was assumed to lie within a few MeV above the $p\Xi^-$ strong breakup threshold. The resonance width was estimated using the P-matrix formalism [7], and the detector response and event reconstruction/analysis effects were estimated using a fast simulation, detector response code. This new simulation tool, FSDR, enables rapid evaluation of relativistic heavy ion detector/reconstruction/analysis capabilities for proposed, new physics programs at RHIC. STAR's sensitivity for detecting a possible $H^{27} \rightarrow p\Xi^-$ resonance decay was studied as a function of pro-

duction rate and Gaussian width. For Gaussian widths of order 2 MeV or less, discovery should be possible if the production rate for $H^{27} \rightarrow p\Xi^-$ into the STAR acceptance is of order 1 per Au + Au central collision event. This production rate is similar in magnitude to coalescence model predictions for bound dibaryons [11]. Greater discovery potential might be achieved if mixed event $p\Xi^-$ backgrounds are constructed and compared to the data, or if significant enhancement due to increased strangeness production and possible QGP formation occurs in the collisions at RHIC energies.

Acknowledgements

This research was supported in part by The U. S. Department of Energy Grant DE-FG03-94ER40845 and The Robert A. Welch Foundation Grant F-604.

References

[1] Particle Data Group, Eur. Phys. J. C **3**, 1 (1998); see pgs. 609-611.

[2] R. L. Jaffe, Phys. Rev. Lett. **38**, 195 (1977); erratum *ibid.* **38**, 617 (1977).

[3] D. P. Goyal, J. N. Misra and A. V. Sodhi, Phys. Rev. D **21**, 607 (1980); S. Aoki *et al.,* Phys. Rev. Lett. **65**, 1729 (1990); S. Aoki *et al.,* Prog. Theor. Phys. **85**, 1287 (1991); K. Imai, Nucl. Phys. A **527**, 181c (1991); J. K. Ahn *et al.,* Phys. Lett. B **378**, 53 (1996); R. W. Stotzer *et al.,* Phys. Rev. Lett. **78**, 3646 (1997); P. Beillière *et al.,* Phys. Lett. B **39**, 671 (1972); G. Wilquet, W. L. Knight, J. G. Guy, S. N. Tovey, J. Canter, A. Mann, J. Schneps, G. Wolsky, D. J. Miller and F. R. Stannard, Phys. Lett. B **57**, 97 (1975).

[4] B. A. Shahbazian, V. A. Sashin, A. O. Kechechyan and A. S. Martynov, Phys. Lett. B **235**, 208 (1990).

[5] J. Belz *et al.,* Phys. Rev. Lett. **76**, 3277 (1996).

[6] R. J. Oakes, Phys. Rev. **131**, 2239 (1963); A. Th. M. Aerts, P. J. G. Mulders and J. J. de Swart, Phys. Rev. D **17**, 260 (1978); J. F. Donoghue, E. Golowich and B. R. Holstein, Phys. Rev. D **34**, 3434 (1986); S.-Q. Xie, J. Phys. G Nucl. Part. Phys. **15**, 287 (1989); and R. L. Jaffe, private communication.

[7] S. V. Bashinsky and R. L. Jaffe, Nucl. Phys. A **625**, 167 (1997).

[8] J. W. Negele, A. Pochinsky and B. Scarlet, Nucl. Phys. B (Proc. Suppl.) **73**, 255 (1999).

[9] R. L. Jaffe and C. L. Korpa, Nucl. Phys. B **258**, 468 (1985); U. Straub, Z.-Y. Zhang, K. Bräuer, A. Faessler and S. B. Khadkikar, Phys. Lett. B **200**, 241 (1988); Y. Iwasaki, T. Yoshie and Y. Tsuboi, Phys. Rev. Lett. **60**, 1371 (1988); M. Oka, Phys. Rev. D **38**, 298 (1988); Y. Koike, K. Shimizu and K. Yazaki, Nucl. Phys. A **513**, 653 (1990).

[10] R. D. Cousins and J. R. Klein, Phys. Rev. D **56**, 1673 (1997).

[11] C. B. Dover, P. Koch and M. May, Phys. Rev. C **40**, 115 (1989).

[12] J. Schaffner-Bielich, R. Mattiello and H. Sorge, e-Print Archive nucl-th/9908043, unpublished, (1999).

[13] A. Jacholkowski *et al.,* WA97 Collaboration, J. Phys. G: Nucl. Part. Phys. **25**, 423 (1999).

[14] R. P. Bickerstaff and B. G. Wybourne, J. Phys. G: Nucl. Phys. **7**, 275 (1981).

[15] STAR Collaboration, J. W. Harris *et al.,* Nucl. Phys. A **566**, 277c (1994); J. W. Harris and B. Müller, Annu. Rev. Nucl. Part. Sci. **46**, 71 (1996); STAR Collaboration, "Conceptual Design Report for the Solenoidal Tracker at RHIC," STAR Publication PUB-5347 (1992), unpublished.

[16] A. Boucham *et al.,* STAR Publication STAR Note 400 (1999), unpublished.

[17] C. Pigot *et al.,* Nucl. Phys. B **249**, 172 (1985).

[18] H. Piekarz, Nucl. Phys. A **450**, 85c (1986).

[19] C. B. Dover and H. Feshbach, Ann. Phys. (N. Y.) **198**, 321 (1990).

[20] N. Kodama, M. Oka and T. Hatsuda, Nucl. Phys. A **580**, 445 (1994).

[21] S. D. Paganis, T. Udagawa, G. W. Hoffmann and R. L. Ray, Phys. Rev. C **56**, 570 (1997).

[22] C. Pruneau, STAR Publication STAR Note 145 (1994), unpublished; J. T. Mitchell and I. M. Sakrejda, STAR Publication STAR Note 190 (1995), unpublished; D. Cebra *et al.,* STAR Publication STAR Note 211 (1995); unpublished.

[23] W. K. Wilson, STAR Publication STAR Note 233 (1996); unpublished.

[24] B. Nilsson-Almqvist and E. Stenlund, Comp. Phys. Comm. **43**, 387 (1987).

[25] K. Werner, Phys. Rep. **232**, 87 (1993).

[26] H. Sorge, H. Stöcker and W. Greiner, Ann. Phys. (N. Y.) **192**, 266 (1989).

[27] K. Geiger, Phys. Rep. **258**, 237 (1995).

[28] T. Ludlam, A. Pfoh and A. Shor, RHIC Workshop I, eds. P. Haustein and C. Woody (Brookhaven, April 1985), BNL-51921; A. Shor and R. Longacre, Phys. Lett. B **218**, 100 (1989).

[29] L. Ray and G. W. Hoffmann, Phys. Rev. C **54**, 2582 (1996); R. L. Ray and G. W. Hoffmann, Phys. Rev. C **60**, 014906 (1999).

[30] I. G. Bearden *et al.,* NA44 Collaboration, Phys. Rev. C **58**, 1656 (1998); H. Appelshäuser *et al.,* NA49 Collaboration, Eur. Phys. J. C **2**, 661 (1998).

Table I: $J^\pi = 0^+, 1^+ \quad Y = 0$ dibaryon constituents of the $\mathbf{8}\otimes\mathbf{8}$ baryon octet – baryon octet direct product space for each irreducible SU(3) flavor representation. The dominant decay modes for each mass range are shown. NN abbreviates "mass of nucleon + nucleon," and similarly for the other baryon-baryon pairs. Weak decays which reduce the number of strange quarks by 1 or 2 are denoted by "ΔS=1" or "ΔS=2," respectively. "S" denotes strong interaction decays. "EM" denotes electromagnetic decays. "S-Iso" indicates strong interaction decays via the small isospin admixtures in the physical states. "S′" indicates that strong interaction decays from the I=1 states are possible to both $N\Xi$ and $\Lambda\Sigma$.

$SU(3)_f$		Mass Range						
Irrep.	$(J^\pi$,I,$I_3)$	NN-NΛ	NΛ-NΣ	NΣ-$\Lambda\Lambda$	$\Lambda\Lambda$-$N\Xi$	$N\Xi$-$\Lambda\Sigma$	$\Lambda\Sigma$-$\Sigma\Sigma$	$> \Sigma\Sigma$
1	0^+ 0 0	ΔS=2	ΔS=1	ΔS=1	S	S	S	S
8	1^+ 0 0	ΔS=2	ΔS=1	ΔS=1	EM	S	S	S
8	1^+ 1 1	ΔS=2	ΔS=1	ΔS=1	ΔS=1	S	S	S
8	1^+ 1 0	ΔS=2	ΔS=1	ΔS=1	EM	S	S	S
8	1^+ 1 -1	ΔS=2	ΔS=1	ΔS=1	ΔS=1	S	S	S
10	1^+ 1 1	ΔS=2	ΔS=1	ΔS=1	ΔS=1	S	S′	S
10	1^+ 1 0	ΔS=2	ΔS=1	ΔS=1	EM	S	S′	S
10	1^+ 1 -1	ΔS=2	ΔS=1	ΔS=1	ΔS=1	S	S′	S
$\overline{\mathbf{10}}$	1^+ 1 1	ΔS=2	ΔS=1	ΔS=1	ΔS=1	S	S′	S
$\overline{\mathbf{10}}$	1^+ 1 0	ΔS=2	ΔS=1	ΔS=1	EM	S	S′	S
$\overline{\mathbf{10}}$	1^+ 1 -1	ΔS=2	ΔS=1	ΔS=1	ΔS=1	S	S′	S
27	0^+ 0 0	ΔS=2	ΔS=1	ΔS=1	S	S	S	S
27	0^+ 1 1	ΔS=2	ΔS=1	ΔS=1	ΔS=1	S	S′	S
27	0^+ 1 0	ΔS=2	ΔS=1	ΔS=1	$\overset{\text{EM,}}{\text{S}-\text{Iso}}$	S	S′	S
27	0^+ 1 -1	ΔS=2	ΔS=1	ΔS=1	ΔS=1	S	S′	S
27	0^+ 2 2	ΔS=2	ΔS=1	ΔS=1	ΔS=1	ΔS=1	ΔS=1	S
27	0^+ 2 1	ΔS=2	ΔS=1	ΔS=1	ΔS=1	$\overset{\text{EM,}}{\text{S}-\text{Iso}}$	$\overset{\text{EM,}}{\text{S}-\text{Iso}}$	S
27	0^+ 2 0	ΔS=2	ΔS=1	ΔS=1	$\overset{\text{EM,}}{\text{S}-\text{Iso}}$	$\overset{\text{EM,}}{\text{S}-\text{Iso}}$	$\overset{\text{EM,}}{\text{S}-\text{Iso}}$	S
27	0^+ 2 -1	ΔS=2	ΔS=1	ΔS=1	ΔS=1	$\overset{\text{EM,}}{\text{S}-\text{Iso}}$	$\overset{\text{EM,}}{\text{S}-\text{Iso}}$	S
27	0^+ 2 -2	ΔS=2	ΔS=2	ΔS=1	ΔS=1	ΔS=1	ΔS=1	S

Table II: Optimum decay channels and mass ranges for $J^\pi = 0^+, 1^+ \quad Y = 0$ dibaryon resonance searches.

$SU(3)_f$ Irrep.	$(J^\pi$,I,$I_3)$	Decay Channels and Mass Ranges (MeV)	Accessible to STAR
1	0^+ 0 0	$\Lambda\Lambda \gtrsim 2231$	Yes
8	1^+ 0 0	$\Lambda\Lambda \gtrsim 2231$; $n\Xi^0 \gtrsim 2254$; $p\Xi^- \gtrsim 2260$	Yes
8	1^+ 1 1	$p\Xi^0 \gtrsim 2253$	
8	1^+ 1 0	$\Lambda\Lambda \gtrsim 2231$; $n\Xi^0 \gtrsim 2254$; $p\Xi^- \gtrsim 2260$	Yes
8	1^+ 1 -1	$n\Xi^- \gtrsim 2261$	
10	1^+ 1 1	$p\Xi^0 \gtrsim 2253$	
10	1^+ 1 0	$\Lambda\Lambda \gtrsim 2231$; $n\Xi^0 \gtrsim 2254$; $p\Xi^- \gtrsim 2260$	Yes
10	1^+ 1 -1	$n\Xi^- \gtrsim 2261$	
$\overline{\mathbf{10}}$	1^+ 1 1	$p\Xi^0 \gtrsim 2253$	
$\overline{\mathbf{10}}$	1^+ 1 0	$\Lambda\Lambda \gtrsim 2231$; $n\Xi^0 \gtrsim 2254$; $p\Xi^- \gtrsim 2260$	Yes
$\overline{\mathbf{10}}$	1^+ 1 -1	$n\Xi^- \gtrsim 2261$	
27	0^+ 0 0	$\Lambda\Lambda \gtrsim 2231$	Yes
27	0^+ 1 1	$p\Xi^0 \gtrsim 2253$	
27	0^+ 1 0	$\Lambda\Lambda$ from 2231 to 2254;[a] $n\Xi^0 \gtrsim 2254$; $p\Xi^- \gtrsim 2260$	Yes
27	0^+ 1 -1	$n\Xi^- \gtrsim 2261$	
27	0^+ 2 2	$\Sigma^+\Sigma^+ \gtrsim 2379$	
27	0^+ 2 1	$p\Xi^0$ from 2253 to 2382;[b] $\Sigma^+\Sigma^0 \gtrsim 2382$	
27	0^+ 2 0	$\Lambda\Lambda$ from 2231 to 2385;[a] $\Sigma\Sigma \gtrsim 2385$	Yes[c]
27	0^+ 2 -1	$n\Xi^-$ from 2261 to 2390;[d] $\Sigma^0\Sigma^- \gtrsim 2390$	
27	0^+ 2 -2	$\Sigma^-\Sigma^- \gtrsim 2395$	

[a] If strong decay via isospin admixture dominates EM decay and resonance remains narrow; otherwise $\Lambda\Lambda$ for mass $\gtrsim 2231$ MeV only.

[b] If strong decay via isospin admixture dominates EM decay and resonance remains narrow; otherwise $p\Xi^0$ for mass $\gtrsim 2253$ MeV only.

[c] $\Lambda\Lambda$ decay channel only.

[d] If strong decay via isospin admixture dominates EM decay and resonance remains narrow; otherwise $n\Xi^-$ for mass $\gtrsim 2261$ MeV only.

Table III: Kinematic acceptance and reconstruction parameters assumed in the analytical and numerical simulations.

Parameter	Value
Transverse momentum acceptance	$p_T > 0.1$ GeV/c
Pseudorapidity acceptance	$\mid \eta \mid \leq 1$
Azimuthal acceptance	$\phi = 0 \rightarrow 2\pi$
Momentum resolution, $\Delta p/p$	2%
TPC track reconstruction efficiency[a]	90%
SVT track reconstruction efficiency[b]	80%
Particle Identification (π,protons)	100%[c]

[a] Time Projection Chamber; main tracking detector for STAR.
[b] Silicon Vertex Tracker and Silicon Strip Detector tracking system for STAR.
[c] Actual value not yet available.

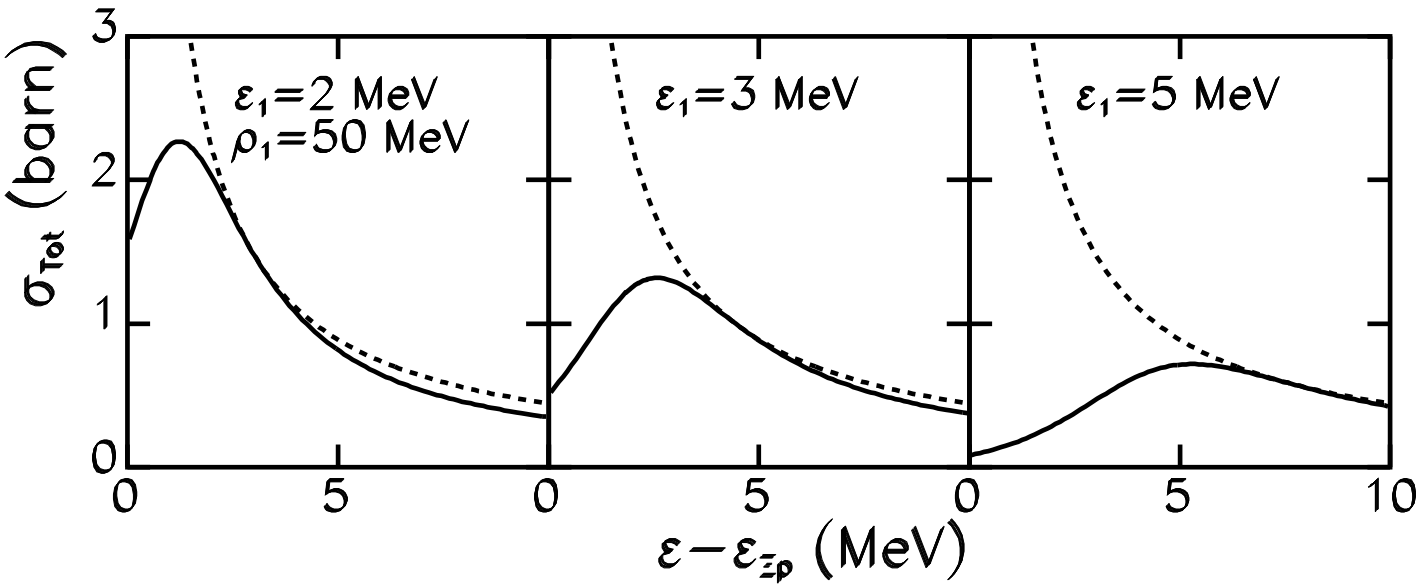

Figure 1: Total elastic cross sections for $N+\Xi$ scattering assuming the H^{27} dibaryon resonance is 2, 3 and 5 MeV above threshold are shown in the left, center and right panels, respectively. The dashed lines indicate the unitarity limit, $4\pi/k_1^2$. The $N\Xi$ threshold energy is denoted by $\varepsilon_{\Xi p}$.

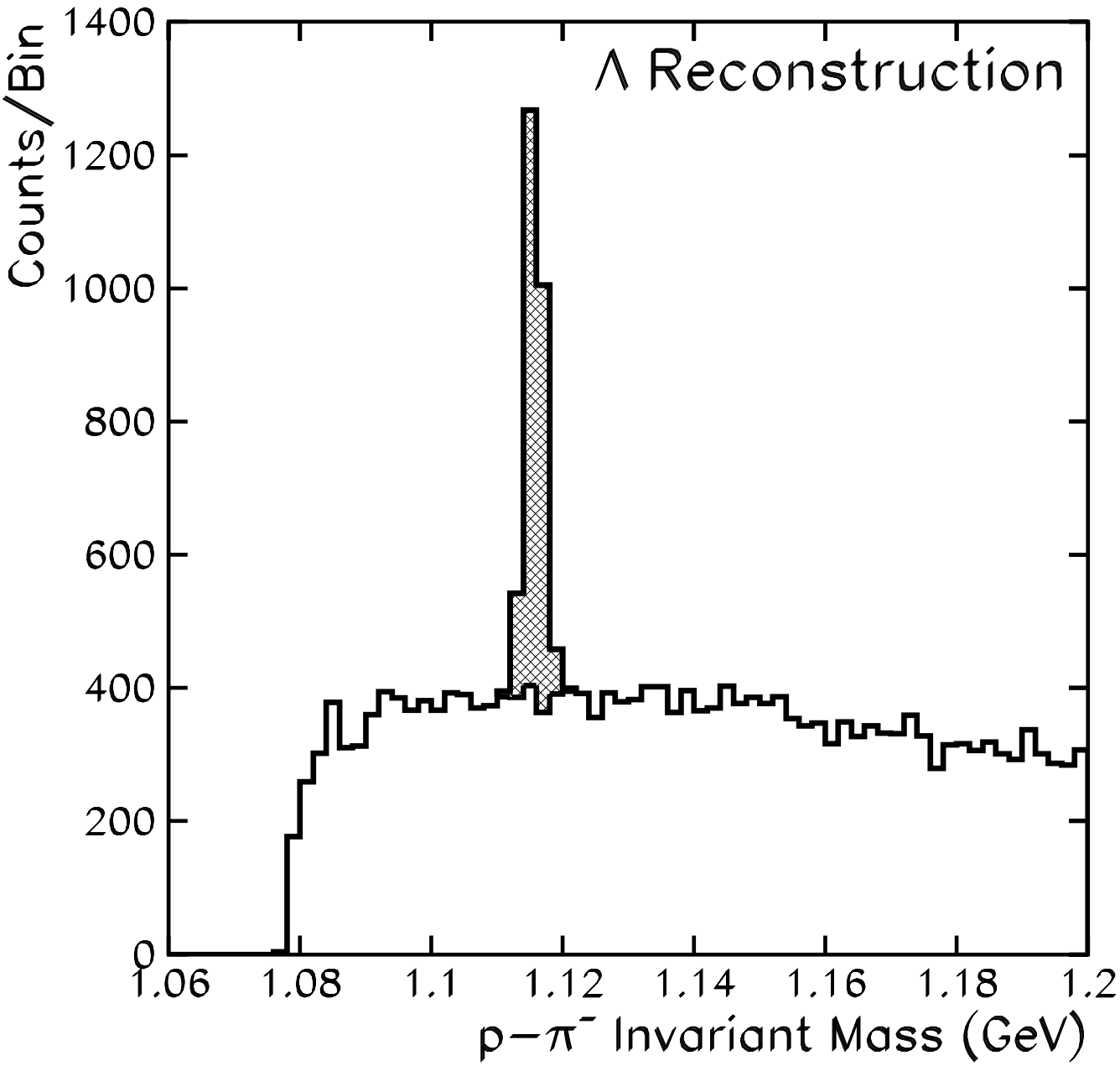

Figure 2: FSDR $p\pi^-$ invariant mass spectrum for $\Lambda \rightarrow p\pi^-$ reconstruction for 600 central Au+Au HIJET events with embedded H^{27} resonances at a collision energy of 200 A·GeV as described in the text. The cross-hatched portion indicates the number of correctly reconstructed $\Lambda \rightarrow p\pi^-$ decays. Bin size is 2 MeV.

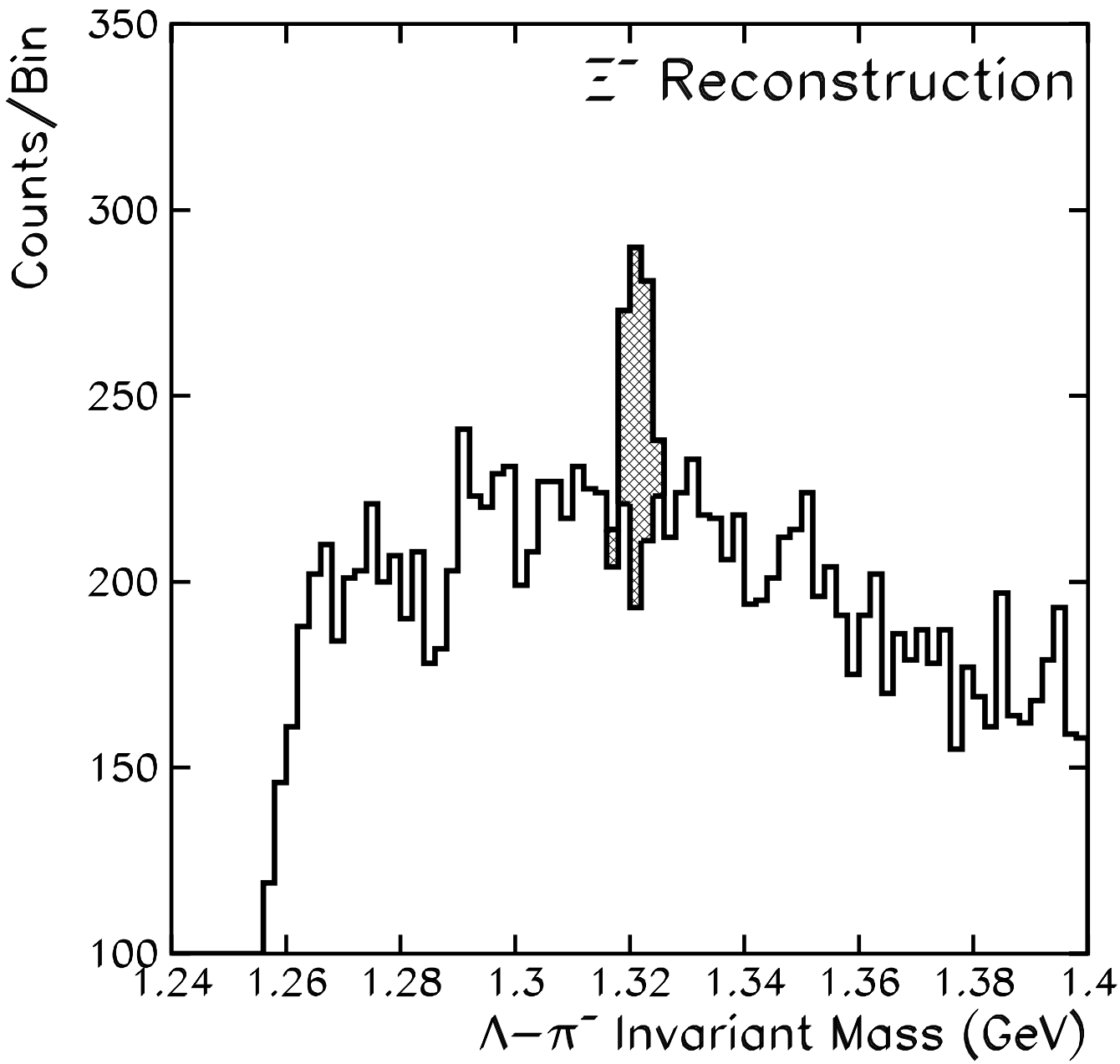

Figure 3: FSDR $\Lambda\pi^-$ invariant mass spectrum for $\Xi^- \rightarrow \Lambda\pi^-$ reconstruction for 600 central Au+Au HIJET events with embedded H^{27} resonances at a collision energy of 200 A·GeV, using the relaxed Ξ^- decay vertex reconstruction cuts described in the text. The cross-hatched portion indicates the number of correctly reconstructed $\Xi^- \rightarrow \Lambda\pi^-$ decays. Bin size is 2 MeV. Note the suppressed zero for the vertical scale.

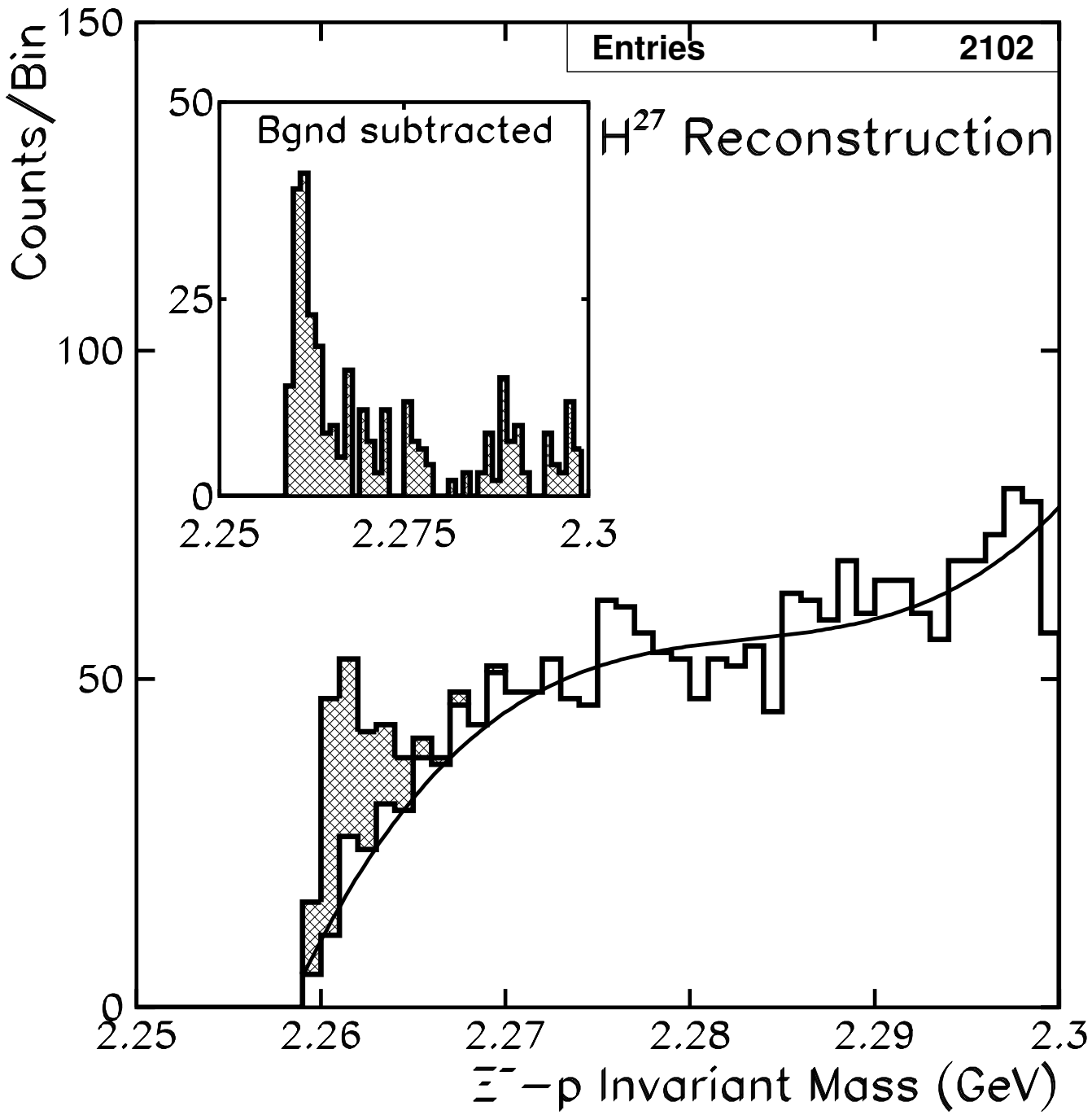

Figure 4: FSDR $p\Xi^-$ invariant mass spectrum for $H^{27} \rightarrow p\Xi^-$ reconstruction for 600 central Au+Au HIJET events at a collision energy of 200 A·GeV, assuming an average of 2.6 $H^{27} \rightarrow p\Xi^-$ resonance decays per event into the acceptance with resonance energy 1 MeV above threshold and Gaussian width parameter (σ) of 2 MeV. The cross-hatched portion indicates the number of correctly reconstructed $H^{27} \rightarrow p\Xi^-$ decays. The background subtracted peak is shown in the inset panel. Bin size is 1 MeV.

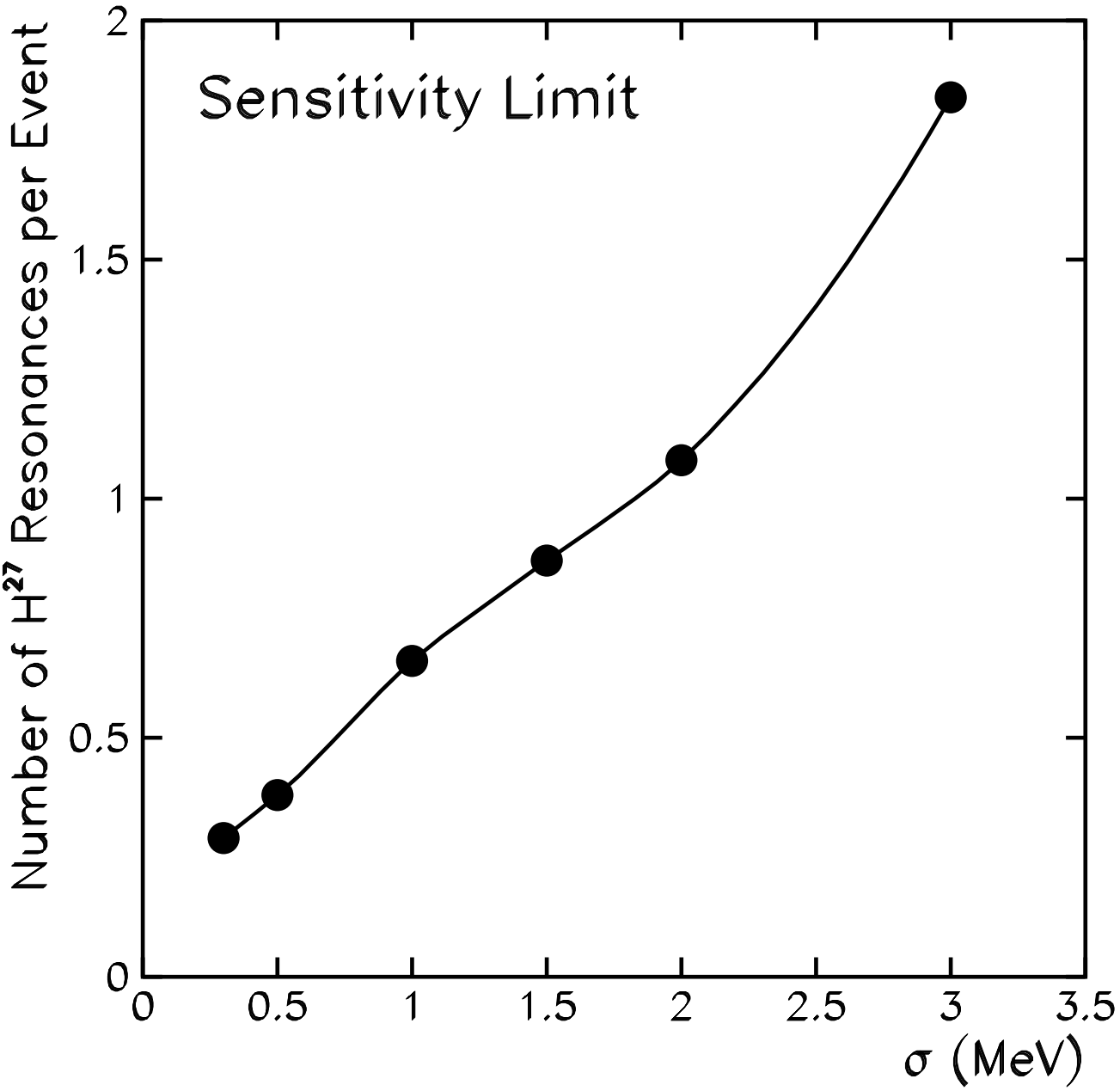

Figure 5: Experimental detection limit based on the reconstruction method described in the text for $H^{27} \rightarrow p\Xi^-$ resonance decays in terms of production rate (number per event into STAR's acceptance) as a function of Gaussian width parameter. Solid dots indicate the cases studied; the line simply connects the dots.